Mathematical Geology, Vol. 38, No. 5, July 2006 (© 2006)
DOI: 10.1007/s11004-006-9030-3

New Indices for Characterizing Spatial Models of Ore Deposits by the Use of a Sensitivity Vector and an Influence Factor[1]

Katsuaki Koike[2] and Setsuro Matsuda[3]

Precise spatial estimation of ore grades and impurity contents from sample data limited in amount and location is indispensable to metallic and nonmetallic resource exploration. One of the advantages of using geostatistics for this purpose is that it can incorporate multivariate data into spatial estimation of one variable. However, there are two weak points concerning technical and post-processing problems. First is the difficulty in application to geologic data in which spatial correlations are not clear because of intrinsic nonlinear behavior. Second is the absence of indices to interpret the mechanisms and factors which govern the spatial distribution. To address these problems, a spatial method of modeling based on a feedforward neural network, SLANS, which recognizes the relationship between the data value and location by considering supplementary attributes such as lithology and biostratigraphy, and a sensitivity analysis using this network were developed. These methods were applied to two case studies, genetic mechanisms of kuroko deposits and quality assessment of a limestone mine. The first case study is a spatial analysis of principal metals of kuroko deposits (volcanogenic massive sulfide deposits) in the Hokuroku district, northern Japan. It was clarified that upward and downward sensitivity vectors were distinguished near the deposits inside and outside the tectonic basin, respectively. Sensitivity analysis for the second case study showed a strong effect of crystalline limestone on the important impurity, P_2O_5 contents. Hydrothermal alteration, which could cause leaching and secondary concentration of phosphorus, is considered to have produced this effect.

KEY WORDS: spatial estimation; sensitivity analysis; influence factor; feedforward neural network; kuroko; limestone.

INTRODUCTION

Spatial modeling techniques must have a high estimation accuracy and should generate realistic alternative images from sample data limited in amount and distribution. As far as a geologic variable which is not a purely random function is concerned, there must be factors that affect its spatial distribution. Such influence

[1]Received 16 April 2004; accepted 30 August 2005; Published online: 26 September 2006.
[2]Department of Civil Engineering, Faculty of Engineering, Kumamoto University, 2-39-1 Kurokami, Kumamoto 860-8555, Japan; e-mail: koike@gpo.kumamoto-u.ac.jp.
[3]Bioinformatics Center, Institute for Chemical Research, Kyoto University, Uji, Kyoto 611-0011, Japan; e-mail: smatsuda@kuicr.kyoto-u.ac.jp.

factors are classified into two categories: physical laws and geological mechanisms. The thermal conductive law, which determines temperature distribution in a media, is representative of the first category. In geological fields, the second type of factors are much more important, because the value or property distribution of a variable is, in general, more complicated than that determined by a physical law. Multivariate analysis is essential for identifying the factors that are helpful in understanding characteristics of the spatial distribution and for estimating its generation process. Therefore, specification of influence factors in addition to pursuit of estimation accuracy is indispensable for spatial modeling of geologic variables. In spite of their importance, there has been much less research on influence factors than on development of spatial modeling techniques.

Such specification can be accomplished by sensitivity analysis of multivariate-based spatial modeling, which is a formalized procedure for identifying the main contributors to model output uncertainty by examining the impact of changes in model inputs on the output. Effective uses of sensitivity analyses are noted in spatial modeling based on GIS, especially in problems related to environments such as air quality (Hwang, Karimi, and Byun, 1998), water quality (Lenhart and others, 2002), eutrophication in shallow water (Pastres and others, 1999), hydrologic models for flooding risk assessment (Crosetto, Tarantola, and Saltelli, 2000), sediment river networks for improving land and water management (Newham and others, 2003), and coastal oil spills (Li, Brimicombe, and Ralphs, 2000). Because most GIS models are constructed through multivariate regression, the spatial variability is smoothed and local changes in the factors cannot be detected by the principle of linear regression. The same situation applies to multivariate geostatistics, which utilize a correlation between two variables using a statistic quantity called a cross-semivariogram. Concurrent incorporation of correlations among many variables into co-kriging is difficult, because many cross-semivariograms must be produced in detailed multivariate analysis, by considering all combinations of variable pairs that possibly have relations. It can be inferred that all the combinations do not necessarily show good spatial correlations. Moreover, there may be cases in which the spatial correlations change locally.

For these problems, we propose the application of a feedforward neural network as Koike, Matsuda, and Gu (2001) and a sensitivity analysis of the network. The network structure and training are the same as Koike and others (2002) and Koike and Matsuda (2003), but the sensitivity analysis is newly developed and discussed in detail in this paper. These methods are applied to two resource exploration case studies, by modeling metal and impurity distributions with a combination of chemical, lithologic, geophysical, and biostratigraphic data in a district and in a limestone mine. Application of geostatistics is inappropriate for both these studies because of a lack of clear spatial correlations in the sample data. The first case study is a spatial analysis of three principal metals of kuroko ores,

Cu, Pb, and Zn, in the Hokuroku district, northern Japan, using the same data set as in Koike and others (2002). The word "kuroko" refers to a massive, compact black ore containing mainly sphalerite, galena, barite, pyrite, and chalcopyrite. Kuroko deposits were formed during the middle Miocene, Nishikurosawa stage, and are hosted in dacite lavas, tuff breccias, and tuffs. The second case study targets the four impurity elements, SiO_2, Fe_2O_3, MnO, and P_2O_5, in an undeveloped limestone mine site covering 2 km E–W and 1.5 km N–S, in southwestern Japan. The data set used is the same as in Koike and Matsuda (2003). Sensitivity vectors and influence factors are proved to be effective for considering occurrence mechanisms of ore deposits and prospecting for high-quality limestone.

SENSITIVITY ANALYSIS FOR NEURAL NETWORK

Feedforward Network with Back-Propagation Learning

Among many possible artificial neural network architectures, a simple feedforward type composed of three layers (input, middle or hidden, and output layers) is adopted here. The network training is based on SLANS (Sequential Learning of Artificial Neural network and Selection of output considering local estimation accuracy: Koike and others, 2002) to avoid overfitting in the network training and consider local distributions of input and output parameters. SLANS identifies the best pair of the numbers of neurons in the middle layer and training data at a sample point by the cross validation method, which calculates the difference between the measured value and estimated value at a sample point using sample data around the point. This processing is based on the idea that network capability probably depends on network structure and both the number and location of training data, and this affects the estimation accuracy of the results. At each target point, the pair nearest the sample point was used for network training.

Figure 1 shows the network for principal metals of kuroko ore in the Hokuroku district. The input layer has neurons corresponding to the (x, y, z) coordinates of sample points and auxiliary information. All the input values are normalized within the range of 0–1 by their minima and maxima. For the kuroko case study, there are 26 auxiliary neurons for Bouguer gravity anomaly and geology classified into 25 rock codes with respect to ages and lithologies. Only one neuron that agrees with the rock present at the point is assigned a 1 and the others are all assigned 0. The same procedure is applied to the limestone case study except that fossil codes are used instead of Bouguer gravity anomaly. Assignment of binary values to the fossil codes is carried out in the same way as for the rock codes. Output data are Cu, Pb, and Zn contents and rock alteration index (AI) related to reactions with hydrothermal fluids for the kuroko case study, and the impurity contents, SiO_2, Fe_2O_3, MnO, and P_2O_5, for the limestone case study.

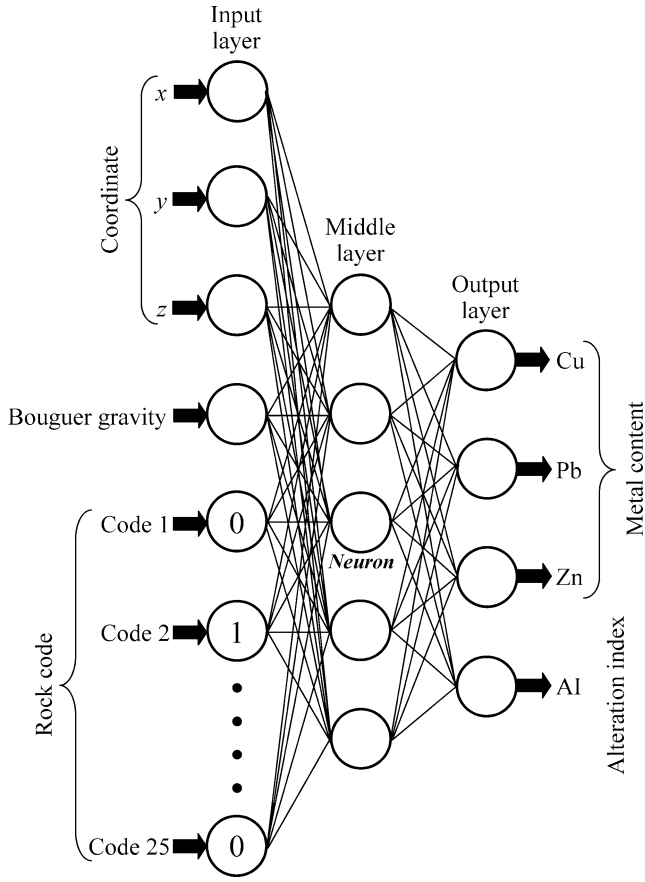

Figure 1. Architecture of artificial neural network composed of three layers used for estimating principal metals of kuroko ore, Cu, Pb, and Zn, in the case study of kuroko deposits.

Weights interconnecting neurons are determined from training data and by an iterative process that minimizes the objective function, E, expressing the total squared error:

$$\left.\begin{aligned} E_p &= \frac{1}{2}\sum_{j=1}^{N}(v_{jp}-o_{jp})^2 \\ E &= \sum_{p=1}^{n}E_p = \frac{1}{2}\sum_{p=1}^{n}\sum_{j=1}^{N}(v_{jp}-o_{jp})^2 \end{aligned}\right\} \tag{1}$$

where p is the learning pattern, o_{jp} is the desired output for p, v_{jp} is the actual output, n is the number of samples in the training data set, and N is the number of neurons in the output layer. Learning continues until E converges to an acceptably small value.

Back propagation, as noted by Rumelhart, Hinton, and Williams (1986), is the most common among the learning algorithms available for adjusting the weight coefficient, $w_{i,j}^{k-1,k}$ between neuron i in layer $k-1$ and neuron j in layer k, and the offset (threshold limit to ignite a neuron), θ_j^k for neuron j in layer k. In back propagation, learning proceeds from the output layer toward the input layer, which is in the opposite direction to signal propagation. This method defines the changes of weight and offset with the progress of learning by:

$$\left.\begin{aligned} \mathrm{w}_{i,j}^{k-1,k}(\tau+1) &= \mathrm{w}_{i,j}^{k-1,k}(\tau) + \Delta \mathrm{w}_{i,j}^{k-1,k}(\tau) \\ \theta_j^k(\tau+1) &= \theta_j^k(\tau) + \Delta\theta_j^k(\tau) \end{aligned}\right\} \tag{2}$$

where τ is the iteration number, and $\Delta w_{i,j}^{k-1,k}(\tau)$ and $\Delta\theta_j^k(\tau)$ are the correction quantities. These quantities can be calculated as:

$$\left.\begin{aligned} \Delta w_{i,j}^{k-1,k}(\tau) &= -\left(\frac{1}{n}\right)\left(\sum_{p=1}^{n} \frac{\partial E_p}{\partial_{w_{i,j}^{k-1,k}}}\right)\eta_w + \Delta w_{i,j}^{k-1,k}(\tau-1)\alpha(\tau) \\ \Delta\theta_j^k(\tau) &= -\left(\frac{1}{n}\right)\left(\sum_{p=1}^{n} \frac{\partial E_p}{\partial\theta_j^k}\right)\eta_\theta + \Delta\theta_j^k(\tau-1)\alpha(\tau) \\ \alpha(\tau) &= \begin{cases} \alpha(\tau-1)+\Delta\alpha, & \text{if} \quad \alpha(\tau-1)+\Delta\alpha < C \\ C, & \text{if} \quad \alpha(\tau-1)+\Delta\alpha \geq C \end{cases} \end{aligned}\right\} \tag{3}$$

where $\eta_w(=0.8)$ and $\eta_\theta(=0.6)$ are the learning rates, $\alpha(\tau)$ is the momentum composed of initial value, $\alpha(1)=0.3$; the step width, $\Delta\alpha=0.01$; and the threshold, $C=0.9$. These values follow the results of learning examination by Koike and others (2002). The partial differential terms of E_p are obtained by:

$$\left.\begin{aligned} \frac{\partial E_p}{\partial w_{i,j}^{k-1,k}} &= -\delta_{jp}^k v_{ip}^{k-1} \\ \frac{\partial E_p}{\partial\theta_j^k} &= -\delta_{jp}^k \\ \delta_{jp}^k &= \begin{cases} -\left(v_{jp}^o - o_{jp}\right)h'\left(u_{jp}^o\right) \\ h'\left(u_{jp}^k\right)\sum_{s=1}^{l_{k+1}} w_{j,s}^{k,k+1}\delta_{sp}^{k+1} \end{cases} \end{aligned}\right\} \tag{4}$$

where v_{jp}^k is the output from neuron j in layer k for p, and $h'(u_{jp}^k)$ is a derivative of the logistic sigmoid function h. The δ_{jp}^k term can be calculated recurrently by using the learning signals of layer $k+1$, δ_{sp}^{k+1} ($s = 1, 2, \ldots, l_{k+1}$; l_{k+1} represents the number of neurons in layer $k+1$) and the following equations:

$$\left.\begin{aligned} u_{jp}^k &= \sum_{i=1}^{l_{k-1}} w_{i,j}^{k-1,k} v_{ip}^{k-1} + \theta_j^k \\ v_{jp}^k &= h\left(u_{jp}^k\right) \end{aligned}\right\} \tag{5}$$

Definition of Influence Factor and Sensitivity Vector

There have been different approaches to sensitivity analysis for neural networks, but their objectives are common: ranking parameters and identifying ones important for simplifying the problem and creating a more compact, optimal network by eliminating unimportant inputs. Sensitivity analyses can be classified into five types based on their concepts.

- Empirical methods that examine output changes by systematic perturbations of inputs (Wei, Sugiura, and Maekawa, 2001), and by changing the numbers of neurons in the input and middle layers (Jarvis and Stuart, 1996).
- Decomposition of the variance of the model output conditioned on the inputs (Marseguerra and others, 2003).
- Sequential zeroing of weight coefficients of the connection between input and middle layers (Andersson, Åberg, and Jacobsson, 2000).
- Differential analysis of the relationship between inputs and output using a Taylor series (Ricotti and Zio, 1999).
- Derivative analysis of the relationship in order to derive the sensitivity coefficient matrix (Engelbrecht, Cloete, and Zurada, 1995; Sung, 1998).

From these five, we selected the derivative type because of its strictness and direct derivation of sensitivity coefficients. Sensitivity analyses of the special cases for networks having one and two middle layers were investigated by Engelbrecht, Cloete, and Zurada (1995) and Sung (1998), respectively, but we extended this to a general form of sensitivity coefficients as follows:

Let v_κ be the output from neuron κ in the output layer (termed O hereafter) and ξ_a be the input to neuron a in the input layer (termed I). The sensitivity coefficient of v_κ with respect to ξ_a, $A_{\kappa a}$ is defined by:

$$A_{\kappa a} = \frac{\partial v_\kappa}{\partial \xi_a} \tag{6}$$

When the neural network consists of three layers, Equation (6) can be decomposed to a partial derivatives form as follows:

$$\frac{\partial v_\kappa}{\partial \xi_a} = \sum_{b=1}^{M} \frac{\partial v_\kappa}{\partial \zeta_b} \cdot \frac{\partial \zeta_b}{\partial \xi_a} \tag{7}$$

where ζ_b is the output from neuron b in the middle layer and M is the number of neurons in it. $\partial v_\kappa / \partial \zeta_b$ on the right side of Equation (7) can be further decomposed to:

$$\frac{\partial v_\kappa}{\partial \zeta_b} = \frac{\partial v_\kappa}{\partial v_\kappa^{(\text{in})}} \cdot \frac{\partial v_\kappa^{(\text{in})}}{\partial \zeta_b} = h'\left(v_\kappa^{(\text{in})}\right) \cdot w_{\kappa b}^{O,1} \tag{8}$$

where $v_\kappa^{(\text{in})}$ is the input to neuron κ in O, and $w_{\kappa b}^{O,1}$ is the weight coefficient connecting neuron κ with neuron b. Similarly, $\partial \zeta_b / \partial \xi_a$ in Equation (7) is rewritten as:

$$\frac{\partial \zeta_b}{\partial \xi_a} = \frac{\partial \zeta_b}{\partial \zeta_b^{(\text{in})}} \cdot \frac{\partial \zeta_b^{(\text{in})}}{\partial \xi_a} = h'\left(\zeta_b^{(\text{in})}\right) \cdot w_{ba}^{1,I} \tag{9}$$

where $\zeta_b^{(\text{in})}$ is the input to neuron b, and $w_{ba}^{1,I}$ is the weight coefficient connecting neuron b with neuron a in I. Substitution of Equations (8) and (9) into Equation (7) produces a new expression for $A_{\kappa a}$:

$$A_{\kappa a} = h'\left(v_\kappa^{(\text{in})}\right) \sum_{b=1}^{M} w_{\kappa b}^{O,1} h'\left(\zeta_b^{(\text{in})}\right) \cdot w_{ba}^{1,I} \tag{10}$$

This equation can be extended to a general form for an arbitrary network that consists of L middle layers with different numbers of neurons, M_i ($i = 1, \ldots, L$):

$$\begin{aligned} \frac{\partial v_\kappa}{\partial \xi_a} &= \sum_{b_L=1}^{M_L} \frac{\partial v_\kappa}{\partial \zeta_{b_L}^L} \left(\sum_{b_{L-1}=1}^{M_{L-1}} \frac{\partial \zeta_{b_L}^L}{\partial \zeta_{b_{L-1}}^{L-1}} \sum_{b_{L-2}=1}^{M_{L-2}} \frac{\partial \zeta_{b_{L-1}}^{L-1}}{\partial \zeta_{b_{L-2}}^{L-2}} \cdots \sum_{b_1=1}^{M_1} \frac{\partial \zeta_{b_2}^2}{\partial \zeta_{b_1}^1} \frac{\partial \zeta_{b_1}^1}{\partial \xi_a} \right) \\ &= \sum_{b_L=1}^{M_L} \sum_{b_{L-1}=1}^{M_{L-1}} \sum_{b_{L-2}=1}^{M_{L-2}} \cdots \sum_{b_1=1}^{M_1} \left\{ \frac{\partial v_\kappa}{\partial \zeta_{b_L}^L} \frac{\partial \zeta_{b_L}^L}{\partial \zeta_{b_{L-1}}^{L-1}} \frac{\partial \zeta_{b_{L-1}}^{L-1}}{\partial \zeta_{b_{L-2}}^{L-2}} \cdots \left(\frac{\partial \zeta_{b_2}^2}{\partial \zeta_{b_1}^1} \frac{\partial \zeta_{b_1}^1}{\partial \xi_a} \right) \right\} \end{aligned} \tag{11}$$

Referring to the relations deduced in Equations (8) and (9), Equation (11) is transformed, in accordance with the manner of Equation (10), into:

$$A_{\kappa a} = \sum_{b_L=1}^{M_L} \sum_{b_{L-1}=1}^{M_{L-1}} \sum_{b_{L-2}=1}^{M_{L-2}} \cdots \sum_{b_1=1}^{M_1} \left[h'\left(v_\kappa^{(\mathrm{in})}\right) w_{\kappa b_L}^{O,L} h'\left(\zeta_{b_L}^{L(\mathrm{in})}\right) w_{b_L b_{L-1}}^{L,L-1} h'\left(\zeta_{b_{L-1}}^{L-1(\mathrm{in})}\right) w_{b_{L-1} b_{L-2}}^{L-1,L-2} \right.$$
$$\left. \times \Lambda \left\{ h'\left(\zeta_{b_2}^{2(\mathrm{in})}\right) w_{b_2 b_1}^{2,1} h'\left(\zeta_{b_1}^{1(\mathrm{in})}\right) w_{b_1 a}^{1,I} \right\} \right] \tag{12}$$

After training the neural network, the values of all weight coefficients are determined. Therefore, the values of the sensitivity coefficients for all neurons in I can be calculated using Equations (10) and (12). The input neuron which has the largest sensitivity coefficient is defined as an influence factor.

Furthermore, we defined the sensitivity vector, ∇v_κ, to extract spatial characteristics of target data. The ∇v_κ of neuron κ in O is composed of the sensitivity coefficients for the (x, y, z) coordinates.

$$\nabla v_\kappa = \left(\frac{\partial v_\kappa}{\partial x}, \frac{\partial v_\kappa}{\partial y}, \frac{\partial v_\kappa}{\partial z} \right)^{\mathrm{T}} \tag{13}$$

In the case of $\nabla v_\kappa = (0, 0, 1)^{\mathrm{T}}$, a small change in the z coordinate strongly affects the κ-th output, while the effects of the x and y coordinates are negligible. Thus, the z coordinate becomes a predominant influence factor for this case.

DETECTING SENSITIVITY VECTOR FEATURES

To understand the meaning of the sensitivity vector, we prepared two reference models, as shown in Figure 2. Both models contain high value zones in the middle areas, which are assumed to be ore bodies, but their shapes are different in that (a) is a cube and (b) is a plate. The value and lithologic distributions in the areas were obtained by referring to the principal metals and geology data from the kuroko case study. Model (a) is assigned by simple distribution, which is composed of 11 (ln ppm: ln denotes natural logarithm) and kuroko-related ores (RC 25 in the figure) in the middle and 4 (ln ppm) and the Miocene dacite (RC 12) surrounding it. In Model (b), the value changes only along the z axis and decreases by 1 (ln ppm) interval from 10 to 5 (ln ppm) in inverse proportion to the distance from the ore body as shown in (c). Lithology also changes from the ores to the Miocene dacite and basalt (RC 19). Both models are divided by cubic meshes with grid-point numbers of (a) $10 \times 10 \times 10$ and (b) $11 \times 11 \times 12$ along the x, y, and z axes. We set a problem: to reconstruct the reference models using 25-% grid point

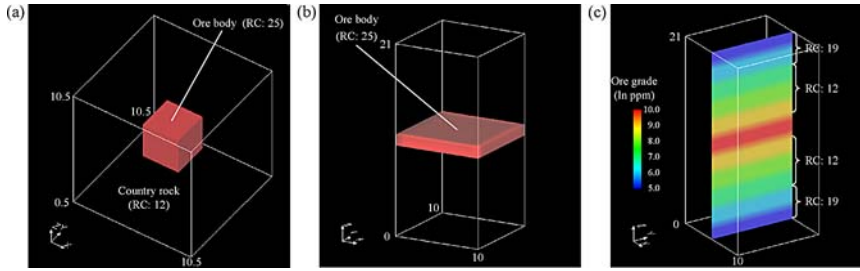

Figure 2. Two reference models differing in ore-body shapes, (a) cubic and (b) planar bodies, used to clarify the meaning of the sensitivity vectors. Values (assumed ore grades) in (b) decrease linearly with distance from the ore body as shown in (c). RC means rock code assigned to ore body and Miocene country rocks.

data selected randomly from the meshed models and SLANS. Bouguer gravity anomaly and AI are not included in this reconstruction.

Figure 3 presents the reconstruction results obtained by extracting only the portions of estimated values larger than (a) 10.6 and (b) 9.6 (ln ppm), and this

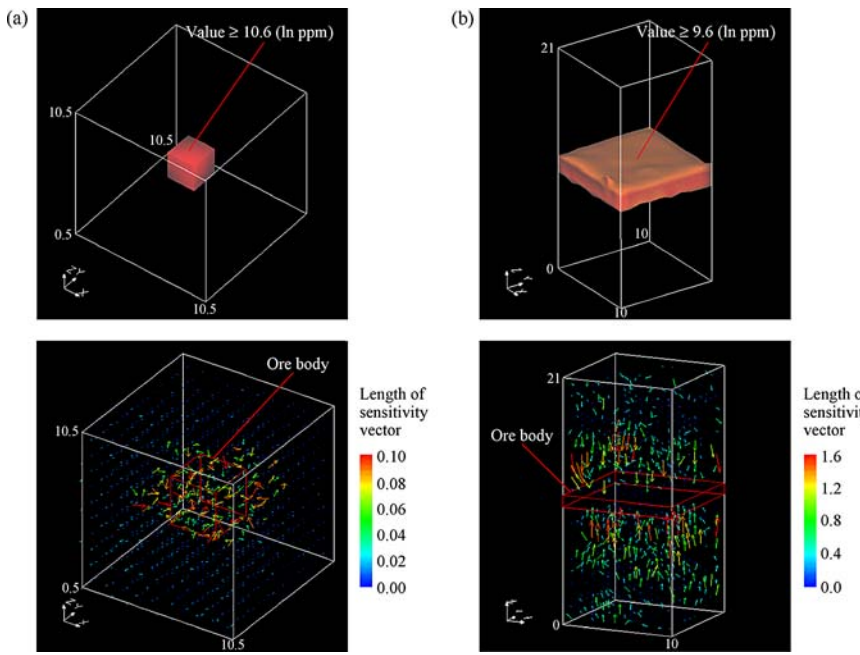

Figure 3. High value zones estimated by SLANS and sensitivity vector maps for Models (a) and (b) in Figure 2.

proves the high estimation ability of SLANS, because the reconstructed ore bodies agree well with the references. The sensitivity vectors in Model (a) become long around the ore body and most point to its center, as shown in Figure 3. Similar trends to these are seen in the sensitivity vectors around the ore body in Model (b), but they are almost parallel to the z axis. Lengths of sensitivity vectors are generally longer than for Model (a), because the spatial variability of values is smaller in Model (a), except for the geologic boundary. Another important feature is that the vector directions are reversed between the upper and lower sides of the ore body: they point to the direction along which the values increase. Consequently, we can detect the characteristics of sensitivity vectors in that they are large in a high variability environment, especially around high value zones, and point to the direction along which the increase ratio of the data maximizes.

APPLYING SENSITIVITY VECTORS TO PRINCIPAL METALS OF KUROKO

Spatial Characteristics of the Principal Metal Data

The data set in the kuroko case study is obtained from 1917 core samples at 143 drillholes, which originate from an investigation of regional geologic structure by the Ministry of International Trade and Industry (MITI, 1983). Figure 4 shows the distribution of the drillhole sites and principal 14 kuroko mines in the 30×30 km^2 study area. Depths of the drillholes ranged from 250–1190 m with an average of 573 m.

Figure 5 represents two experimental semivariograms, $\gamma(h)$s, of the Cu, Pb, and Zn data transformed into natural logarithms with different directions: vertical and horizontal $\gamma(h)$s along the four directions at 45° intervals. It is obvious that the vertical $\gamma(h)$ of each element shows an unusual trend that is common to all three. The semivariances are large at any separation distance between a sample pair, and almost the same as the variance of data, even when the distances are small. Similarly, the horizontal $\gamma(h)$s have common characteristics with respect to the three elements: they fluctuate greatly around the variances and take their maximum values at short distances. These vertical and horizontal features also are found in experimental cross-semivariograms produced from the two kinds of metal data (Koike and others, 2002). These $\gamma(h)$s demonstrate nonlinear behavior of the sample data, which means that even data located near each other do not have similar values. Therefore, analyzing the data by geostatistical techniques is not meaningful. Part of the complex metallogenesis of kuroko deposits can be confirmed through the characteristics of $\gamma(h)$s.

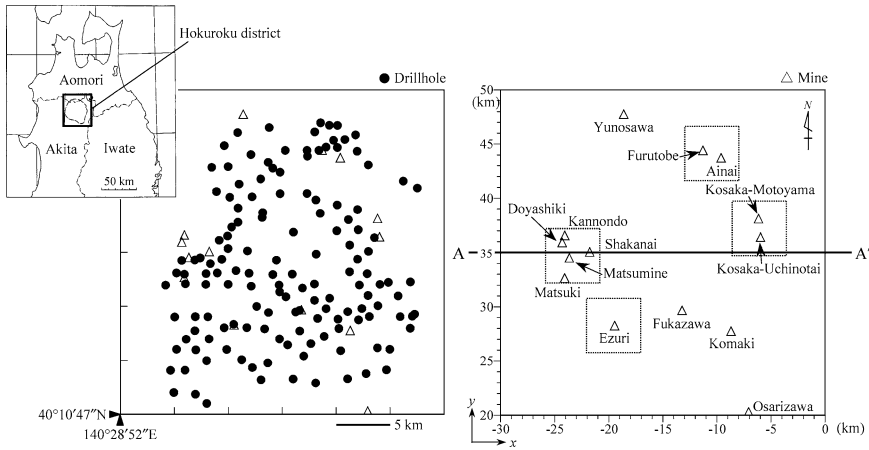

Figure 4. Distributions of 143 drillhole sites from MITI (1983) and principal kuroko mines in the Hokuroku district, northern Japan. Four rectangular areas show the targets for sensitivity vector mapping and semivariogram analysis in Figures 6 and 7. Location in the study area is expressed using the tenth plane rectangular coordinate system of Japan.

Sensitivity Vectors and Discussion

Based on the neurons in the input layer, there are 29 possible influence factors (see Fig. 1). Matsuda and Koike (2003) identified the strong overall influence of the z coordinate common to the three metals. That influence factor appears near the kuroko deposits and faults, and has continuities in a vertical direction. The characteristic indicates that the metals vary largely along this direction. Other important characteristics are that the strength of the influence of lithology differed depending on the metal, and Bouguer gravity anomaly, which is related to structures of basement rocks, had a relatively strong influence.

In addition to the influence factors, sensitivity vectors are also effective in characterizing metal distributions in the Hokuroku district. Four kuroko-deposit areas covering 5 km E–W and 5 km N–S as shown by squares in Figure 4—Hanaoka, including five mines (Matsuki, Matsumine, Shakanai, Doyashiki, and Kannondo), Kosaka, Furutobe and Ainai, and Ezuri—were selected to demonstrate how the sensitivity vectors are applied to detect spatial correlation structures in small regions. The depth ranges of the four areas were defined as 450, 230, 310, and 90 m, respectively, by considering the depth locations and magnitudes of the deposits included in them. Figure 6 shows the sensitivity-vector maps for Zn at the estimation points whose intervals are 500 m and 10 m in the horizontal and vertical directions, respectively. The vertical vectors upward and downward are predominant in the Hanaoka and Kosaka areas, respectively, while the downward

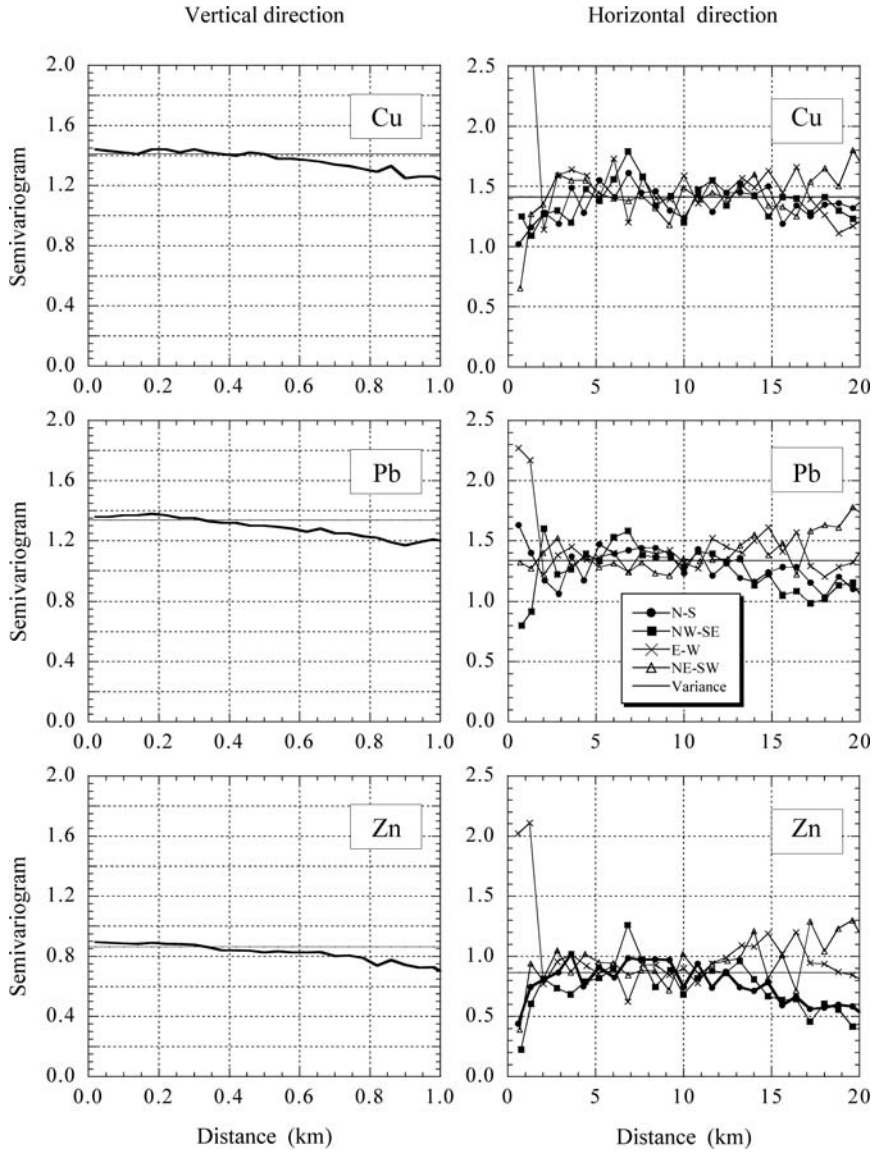

Figure 5. Experimental semivariograms of Cu, Pb, and Zn data transformed into natural logarithms for the vertical and four horizontal directions.

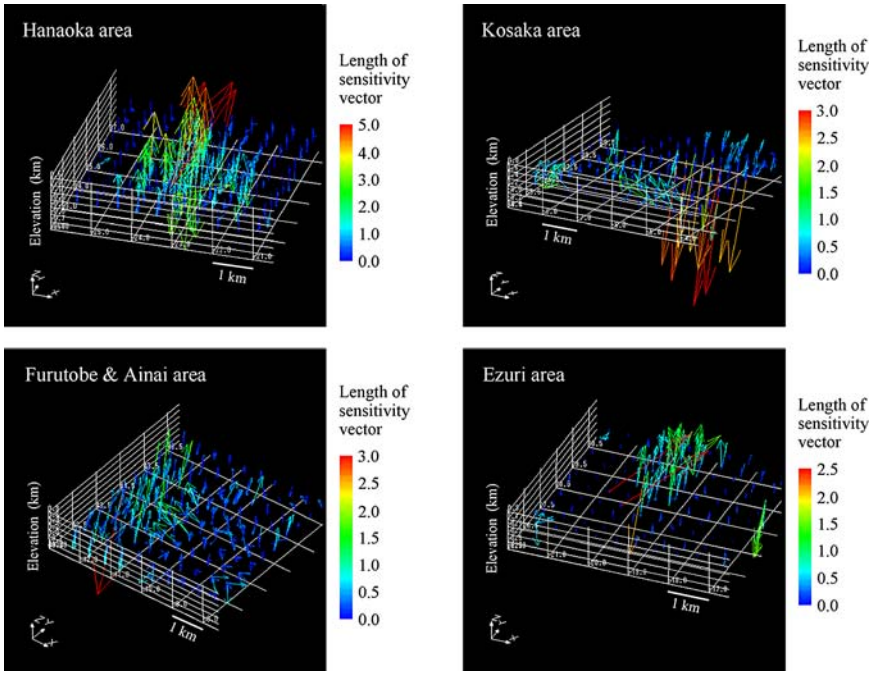

Figure 6. Distributions of sensitivity vectors for Zn in kuroko-mine areas. The locations of areas are shown in Figure 4.

vertical vectors and horizontal vectors pointing to WSW in the Furutobe and Ainai area, and the horizontal vectors pointing to NE in the Ezuri area, are relatively large.

To clarify the relationship between $\gamma(h)$ and the sensitivity vectors, $\gamma(h)$s were produced using the sample data located in the range of 5 km from the center of the defined areas. Directional $\gamma(h)$s along 45° orientations in total—vertical, 4 horizontal (N–S, NE–SW, E–W, and NW–SE), and 40 inclinations (45° rotation steps in the horizontal and 15° dip steps)—were examined, to extract anisotropy of metal distributions in detail. As a result, characteristic $\gamma(h)$s expressing the existence of spatial correlations were obtained along the orientations shown in Figure 7, which are the vertical in the Hanaoka, Kosaka, and Furutobe and Ainai areas and the horizontal NE–SW in the Ezuri area. The $\gamma(h)$s for the Cu, Pb, and Zn data show almost identical patterns, except for the Furutobe and Ainai area, where the $\gamma(h)$ for the Zn is smooth because of the distinct spatial correlations. Those orientations correspond to the dominant directions of the sensitivity vectors, and therefore, the sensitivity vectors can contribute to detecting the direction of the principal axis of the correlations. Focusing on the same metal, the $\gamma(h)$s

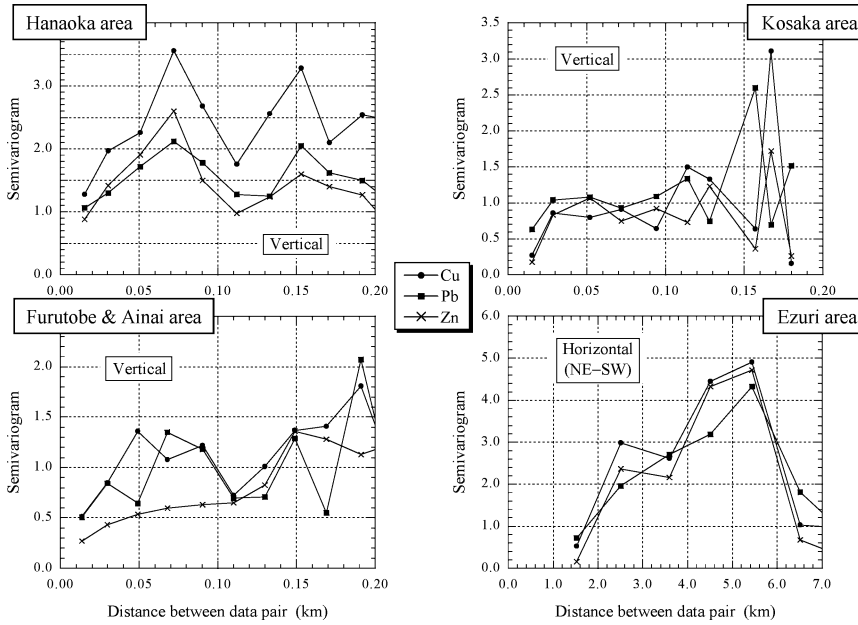

Figure 7. Directional experimental semivariograms using the sample data located in and around the kuroko-mine areas in Figure 4.

differ between the areas. The $\gamma(h)$s indicate that the distances containing spatial correlations are small, 50–150 m in the vertical or about 5 km in the horizontal. Such changeability of $\gamma(h)$ and shortness of the correlation length can account for the $\gamma(h)$s in Figure 5 which show pure nugget type.

In the next step, we used the sensitivity vectors to consider the genetic mechanism of kuroko deposits by classifying the vectors, based on their dips, into three directions: upward, downward, or horizontal. Figure 8 shows the locations and directions of the estimation points at which the magnitudes of the vectors exceed 2.0. The most noteworthy feature is found in large upward and downward vectors concentrated near kuroko deposits inside and outside of the Hanawa-Ohdate area defined in Figure 8, except near the Haboyasan uplift. A hypothesized genetic mechanism was proposed by Matsuda and Koike (2003) based on the solubility of metal sulfide: that the deposits outside the area were formed below the sea floor with the rapid seepage of sea water, and that the deposits inside the area were formed with ore solutions rising through fractures to the sea floor. The local compressive and tensile stress fields can explain the differences in the permeability of fractures through which the ore solutions rose. A pressure decrease of the felsic magma chamber might have caused the stress fields. More details are described in Matsuda and Koike (2003).

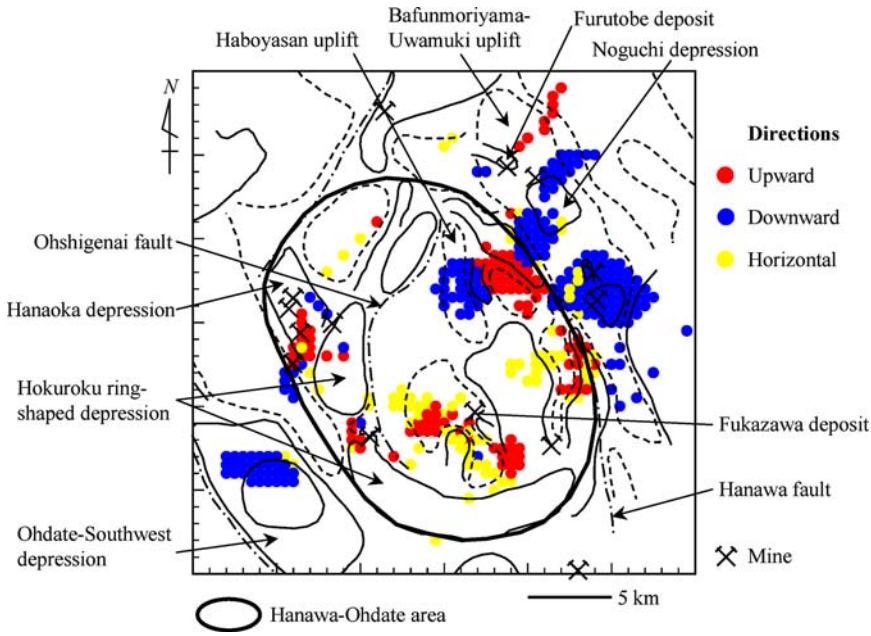

Figure 8. Distribution of estimation points at which the sensitivity vectors are larger than 2.0. Colors of the points represent the directions of the sensitivity vectors.

UTILIZING INFLUENCE FACTORS FOR IMPURITIES IN LIMESTONE

Spatial Modeling of Impurity Contents

Quality control and maintenance of limestone as a resource is of utmost importance, and special attention is paid to the amounts of calcium oxide (CaO) and impurities, which determine the suitability of limestone for industrial use. The purpose of applying sensitivity analysis to impurity distributions in a limestone mine is to understand the mechanism of the concentration process of impurities. The study area is underlaid with Carboniferous and Permian limestone. From 244 sample points at 18 drillhole sites (shown in Fig. 10), data were collected for SiO_2, Fe_2O_3, MnO, and P_2O_5. Figure 9 shows the experimental $\gamma(h)$s using the data transformed into natural logarithms along E–W in the horizontal plane and the vertical direction. E–W is the most reliable direction along which many data pairs can be made because of the drillhole-site distributions. The $\gamma(h)$s signify the absence of distinct spatial correlations of impurities in the study area.

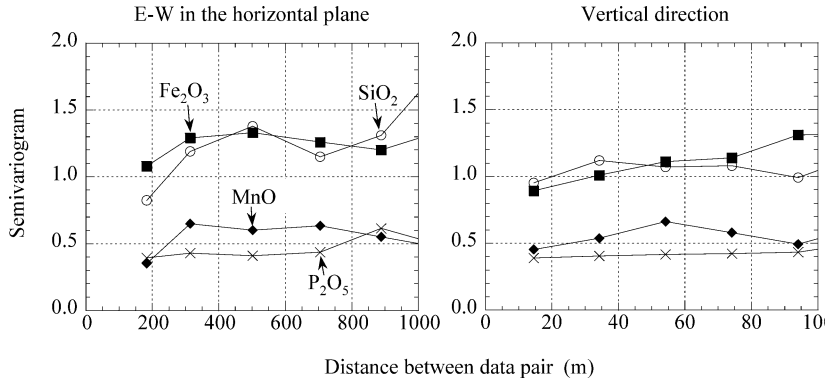

Figure 9. Experimental semivariograms using the sample data of impurity contents transformed into natural logarithms along E–W in the horizontal plane and the vertical direction.

Three kinds of spatial models on geology, fossil zones, and impurity contents were constructed from the ground surface to a depth of 150 m using a uniform grid with intervals of 50 m and 5 m in the horizontal and vertical directions, respectively, by Koike and Matsuda (2003). Figure 10 depicts the horizontal cross-section at the 30 m depth and vertical cross-sections trending E–W (A-A′) and N-S (C-C′) of the impurity distributions determined by SLANS. In these figures, the four chemical content ranges were selected to specify the characteristics of content distribution. A continuity of low content zones of SiO_2 is conspicuous along NE–SW and these correspond with the Lower Permian biostratigraphic zone. The contents of Fe_2O_3 and MnO are similar in that high content zones are distributed in the middle of the study area trending NW–SE and are in contact with low content zones near the western boundary. The P_2O_5 contents have different characteristics from the others in that the northeastern contents are relatively high. The E–W cross-sections show that high contents of Fe_2O_3 and MnO are chiefly distributed in the middle valley. As illustrated in the N–S cross-sections, high SiO_2 and P_2O_5 contents are located at shallow depths near the southern boundary.

Influence Factors and Discussion

Because the ranges of impurity contents are much smaller than those of the metals in the Hokuroku district and there are no anomaly zones such as deposits, the sensitivity vectors are all small and featureless. They cannot be used for a limestone case study.

There are 17 input data, 3 for (x, y, z) coordinates, 9 for lithologies such as conglomeratic, compact, crystalline, and dolomitic limestones, and 5 for fossil zones with different geologic ages. Therefore, 17 influence factors are obtained.

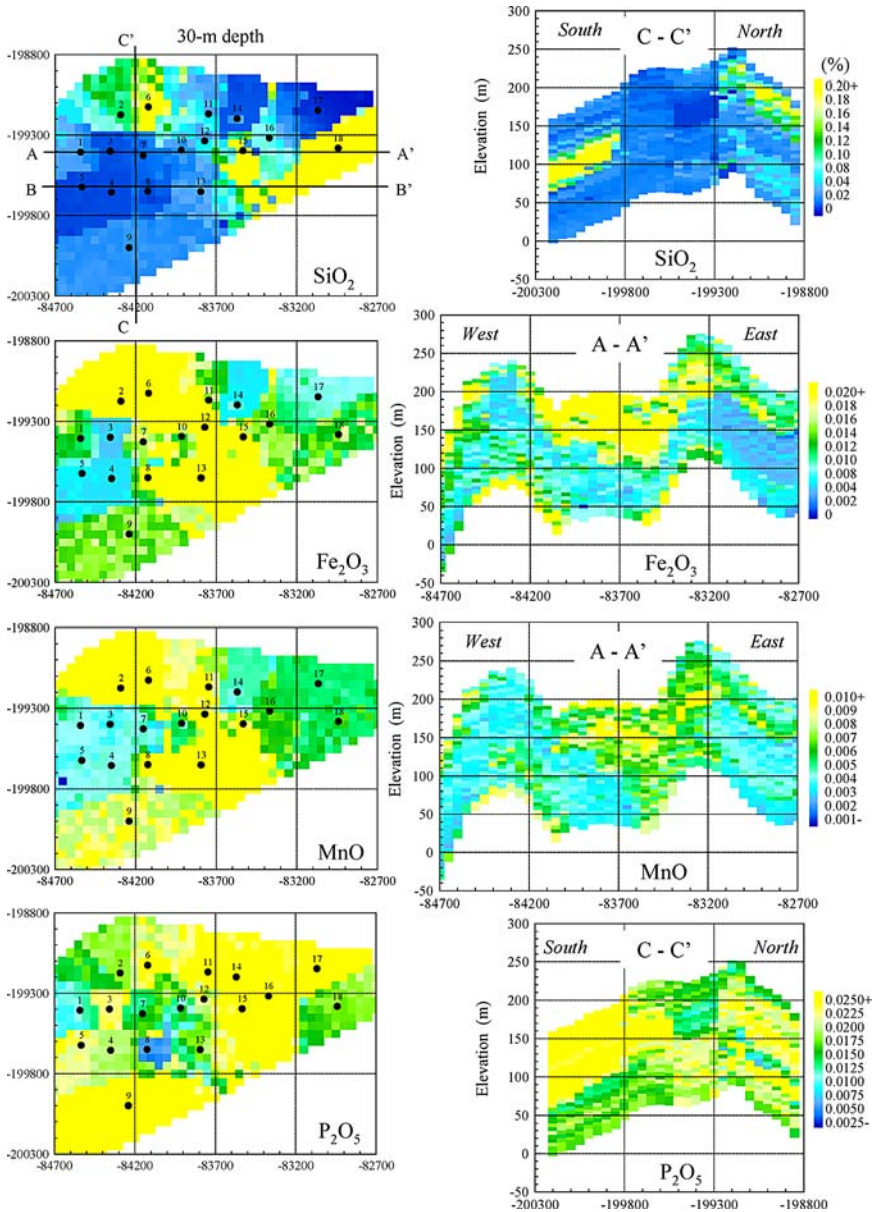

Figure 10. Horizontal cross-sections of SiO_2, Fe_2O_3, MnO, and P_2O_5 contents estimated by SLANS at a depth of 30 m from the ground surface, and their vertical cross-sections along N–S and E–W lines. The distribution of 18 drillhole sites is superimposed on the horizontal cross-sections. Locations in the study area are expressed using the second plane rectangular coordinate system of Japan.

This number is too large to allow characterization of the distributions of influence factors. Thus, we roughly classified the influence factors into four classes, in which the factors are, A: one of the (x, y, z) coordinates, B: one of the lithologies except for crystalline limestone, C: one of the fossil zones, and D: crystalline limestone or absence of fossil. Figure 11 shows the horizontal and vertical slices of the distributions of the four classes for each impurity element at all the estimation points. In the horizontal cross-section at the 30-m depth, Classes C and D are concentrated in the northwestern and southern parts, respectively, common to the four impurities. Clusters of Class D continue up to the 90-m depth for SiO_2 and P_2O_5. Eastern half parts are dominated by Class A for SiO_2 and Fe_2O_3. As shown in the vertical cross-sections along E–W (B-B′) and N–S (C-C′), Class D is remarkably shallower than the 90 m depth, and concentrated in the southwestern parts for SiO_2 and P_2O_5, and in the valleys in the middle parts for Fe_2O_3 and MnO. Another characteristic is that there are remarkable clusters of the same classes at shallow depths, but the classes seem randomly distributed at deep depths.

Table 1 summarizes the ratios of estimated contents satisfying the criteria for high-quality limestone, which are less than 0.1% (SiO_2), 0.05% (Fe_2O_3), 0.01% (MnO), and 0.05% (P_2O_5). Class D has the lowest quality of limestone, and it is noteworthy that the P_2O_5 contents are higher than in the other classes. Industrial uses of limestones change with small differences in the P_2O_5 contents. Accordingly, it is important to pay considerable attention to the distributions of crystalline limestones that constitute Class D influence factors in the design and planning of limestone mining.

The differences between the four classes are detected from the frequency distributions of the contents. Figure 12 compares the histograms of the estimated contents in Classes A and D; those for Classes B and C are similar to those for Class A. It is noteworthy that Class D has bimodal distributions for all the impurities, and this bimodality is remarkable for SiO_2 and P_2O_5. Bimodality is not seen in the histograms of the sample data for the crystalline limestones due to the small amount of data, which proves the significance of detecting influence factors.

To specify the locations of estimation points belonging to Class D, a spatial map for the P_2O_5 and Fe_2O_3 contents was produced, as shown in Figure 13. The spheres and their colors represent the locations of Class D, and estimated contents, respectively. The Class D distributions show a general trend corresponding with the crystalline limestones interbedded along ENE–WSW, according to the geologic model by Koike and Matsuda (2003). The most distinguishing feature is that the distributions are clearly divided into the high and low content zones, with the concentration of low contents in the middle parts. In contrast to P_2O_5, the estimated contents of Fe_2O_3 are scattered, which causes the unclearness of the bimodality in the histogram.

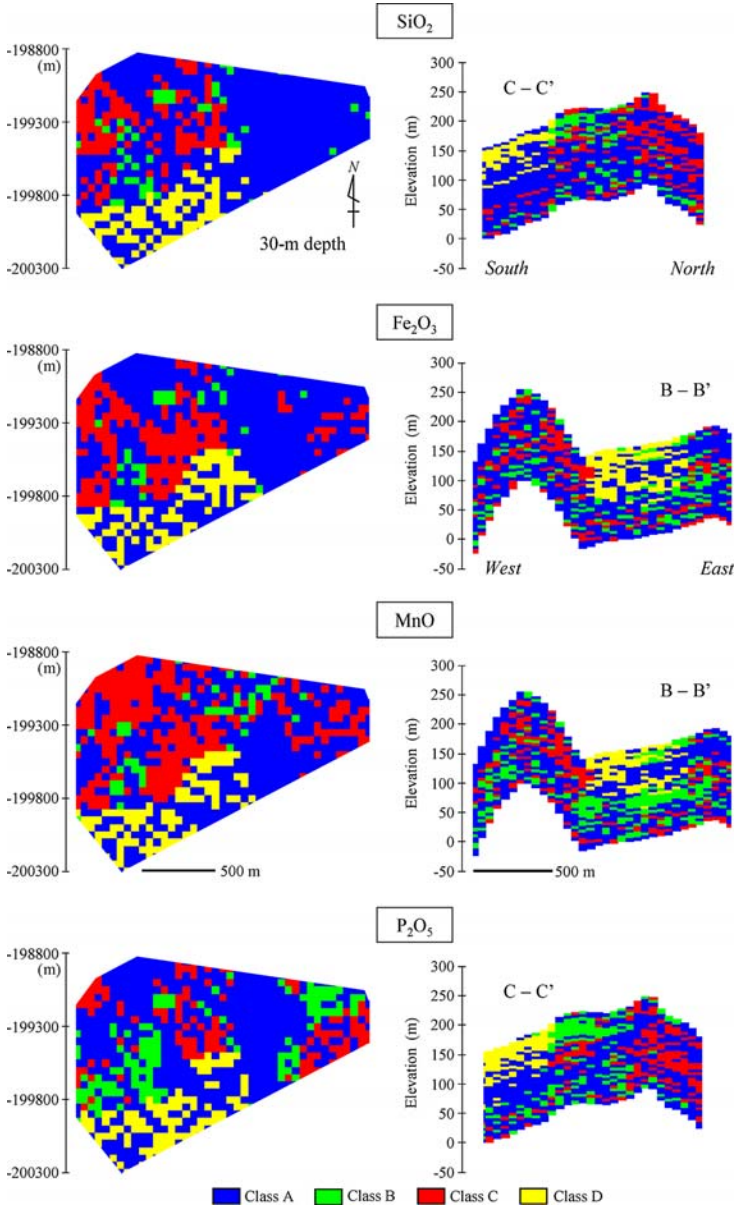

Figure 11. Horizontal and vertical cross-sections of the distributions of four classes whose main influence factors are A: coordinate, B: geology, C: fossil zone, and D: crystalline limestone. The target depth is 30 m. Positions of vertical cross-sections are shown in Figure 10.

Table 1. Percentages of Estimated Contents that Satisfy the Criterion for High-Quality Limestone in Each Influence-Factor Class

Element	SiO_2 (%)	Fe_2O_3 (%)	MnO (%)	P_2O_5 (%)
Criteria	<0.1	<0.05	<0.01	<0.05
Class A	90.5	95.6	93.8	96.3
Class B	94.3	97.2	93.0	96.9
Class C	92.3	89.0	83.9	95.3
Class D	87.9	77.4	69.6	70.4

The four classes are further characterized from a spatial correlation viewpoint. Figure 14 compares horizontal $\gamma(h)$s along the four directions using the estimated P_2O_5 contents in each class, which demonstrates that the spatial correlation structures also vary, depending on the influence factors, as follows:

- Class A: Directional differences of $\gamma(h)$s are the smallest among the four classes, but it has slightly better spatial correlations over long distances along N–S.

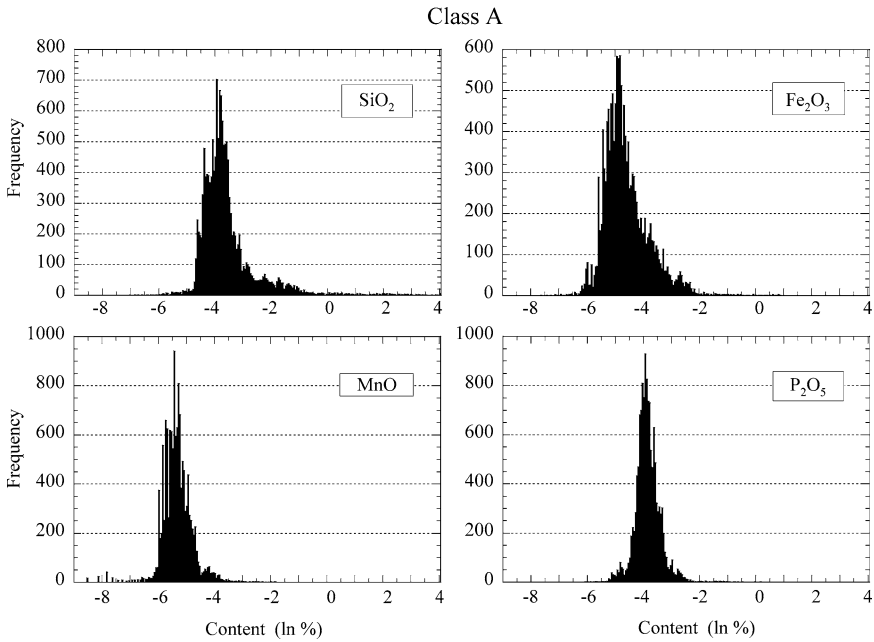

Figure 12. Histograms of estimated contents of the four impurities belonging to the influence-factor classes A and D.

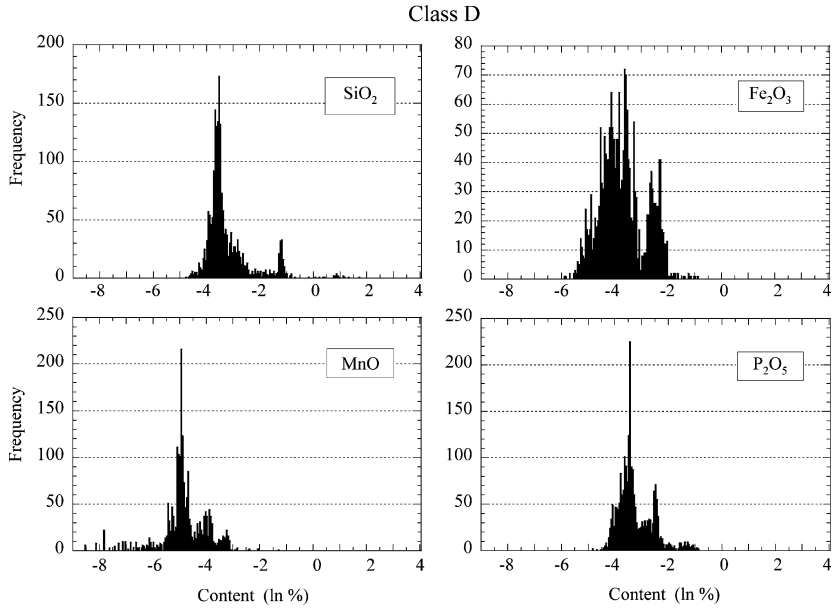

Figure 12. Continued.

- Class B: Weak directional anisotropy is shown, and the $\gamma(h)$ along NW–SE, which is the major axis of the directions of conglomeratic and compact limestone blocks in the study area, has a similar trend to the N–S trend in Class A.

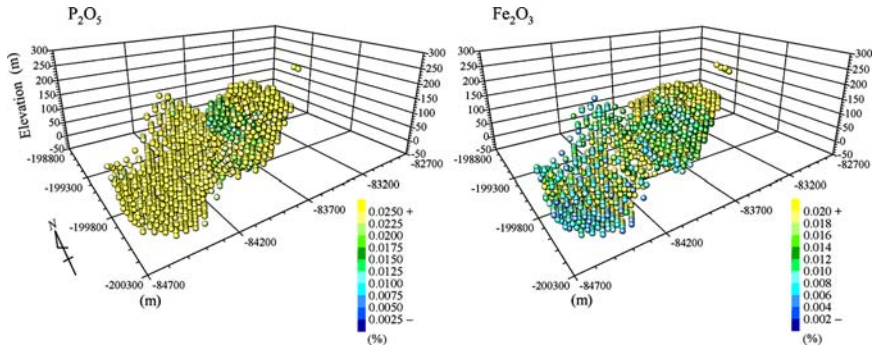

Figure 13. Locations of points belonging to Class D and estimated contents by SLANS for P_2O_5 and Fe_2O_3.

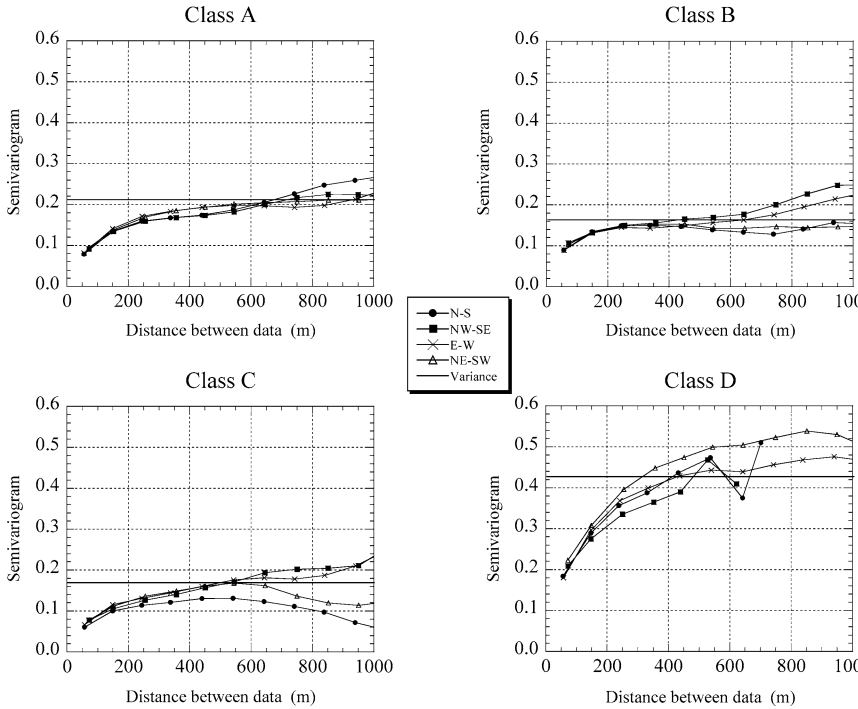

Figure 14. Horizontal semivariograms along the four directions of the estimated P_2O_5 contents in the four classes.

- Class C: Anisotropy is remarkable because the differences in $\gamma(h)$s between NW–SE and N–S are large. NW–SE is the general trend of the Upper Carboniferous and Lower Permian fossil zones, according to the fossil zone model by Koike and Matsuda (2003).
- Class D: Spatial correlations are the most clearly expressed with long correlation lengths, as seen in that the P_2O_5 contents have correlations over 900 m along NE–SW and E–W.

Furthermore, we present a hypothesis on the occurrence of the above bimodality and spatial correlations. It can be inferred from a geological viewpoint that low P_2O_5 is a primary ingredient mixed with soft lime mud. Subsequent leaching of phosphorus from limestones and shales, by hydrothermal alteration accompanied mainly by intrusions of igneous rocks, and secondary concentration of phosphorus, might have produced zones of high P_2O_5 content. Due to high temperatures and rapid flow velocities, hydrothermal fluids could activate the leaching and secondary concentration more efficiently than rainwater. Such secondary concentrations have not been reported for the other impurities, as

estimated from the distributions of Fe_2O_3 contents in Figure 13. Intrusions of igneous rocks are not observed in the study area, but there are outcrops of Cretaceous granodiorite and quartz porphyry around the crystalline limestones. Consequently, hydrothermal alteration of the limestones can be considered as the most important factor determining the quality of limestone, especially P_2O_5 content distributions.

CONCLUSION

As an alternative method for detecting spatial characteristics of geologic variables in detail, sensitivity analysis for a feedforward neural network was proposed and applied to two case studies related to metallic and nonmetallic resource exploration. Although spatial correlations of the data sets were ambiguous, local and divisional correlation structures could be identified using the sensitivity vectors and influence factors. The main results can be summarized as follows.

1. Sensitivity vectors were defined using the sensitivity coefficients for the (x, y, z) coordinates at sample or estimation points. A study on the meaning of sensitivity vectors using ore-body models clarified that the sensitivity vector becomes large in a high variability environment, especially around high value zones, and points to the direction along which the increase ratio of the data maximizes.
2. Semivariogram analysis of principal metal data in the small kuroko-deposit areas demonstrated that the sensitivity vectors were effective at detecting local anisotropy of spatial distributions of the target data with large variability. The directions of the sensitivity vectors helped elucidate the genetic mechanism of kuroko deposits.
3. Influence factor was defined as the input data that has the largest sensitivity coefficient. A case study on applying detection of influence factors to impurity content distributions in a limestone mine clarified that the low-quality portions were strongly affected by crystalline limestones, and the contents of SiO_2 and P_2O_5 in them had distinct bimodality. Hydrothermal alteration accompanied mainly by intrusions of igneous rocks in limestones can be important in activating leaching and secondary concentration of phosphorous.

REFERENCES

Andersson, F. O., Åberg, M., and Jacobsson, S. P., 2000, Algorithmic approaches for studies of variable influence, contribution and selection in neural networks: Chemometr. Intell. Lab. Syst., v. 51, no.1, p. 61–72.

Crosetto, M., Tarantola, S., and Saltelli, A., 2000, Sensitivity and uncertainty analysis in spatial modeling based on GIS: Agric. Ecosyst. Environ., v. 81, no.1, p. 71–79.

Engelbrecht, A. P., Cloete, I., and Zurada, J. M., 1995, Determining the significance of input parameters using sensitivity analysis, From natural to artificial neural computation: Proceedings of International Workshop on Artificial Neural Networks, Malaga-Torremolinos, Spain, p. 382–388.

Hwang, D., Karimi, H. A., and Byun, D. W., 1998, Uncertainty analysis of environmental models within GIS environments: Comput. Geosci., v. 24, no. 2, p. 119–130.

Jarvis, C. H., and Stuart, N., 1996, The sensitivity of a neural network for classifying remotely sensed imagery: Comput. Geosci., v. 22, no. 9, p. 959–967.

Lenhart, T., Eckhardt, K., Fohrer, N., and Frede, H.-G., 2002, Comparison of two different approaches of sensitivity analysis: Phys. Chem. Earth, v. 27, nos. 9/10, p. 645–654.

Koike, K., Matsuda, S., and Gu, B., 2001, Evaluation of interpolation accuracy of neural kriging with application to temperature-distribution analysis: Math. Geol., v. 33, no. 4, p. 421–448.

Koike, K., Matsuda, S., Suzuki, T., and Ohmi, M., 2002, Neural network-based estimation of principal metal contents in the Hokuroku District, northern Japan, for exploring kuroko-type deposits: Nat. Resour. Res., v. 11, no. 2, p. 135–156.

Koike, K., and Matsuda, S., 2003, Characterizing content distributions of impurities in a limestone mine using a feedforward neural network: Nat. Resour. Res., v. 12, no. 3, p. 209–223.

Li, Y., Brimicombe, A. J., and Ralphs, M. P., 2000, Spatial data quality and sensitivity analysis in GIS and environmental modeling: the case of coastal oil spills: Comput. Environ. Urban Syst., v. 24, no. 2, p. 95–108.

Marseguerra, M., Masini, R., Zio, E., and Cojazzi, G., 2003, Variance decomposition- based analysis via neural networks: Reliab. Eng. Syst. Saf., v. 79, no. 2, p. 229–238.

Matsuda, S., and Koike, K., 2003, Sensitivity analysis of a feedforward neural network for considering genetic mechanisms of kuroko deposits: Nat. Resour. Res., v. 12, no. 4, p. 291–301.

MITI, 1983, Report of regional investigations for 1982 (FY): General investigation for structural analysis: Ministry of International Trade and Industry and Agency of Natural Resources and Energy, Tokyo, Japan, 621 p. (in Japanese).

Newham, L. T. H., Norton, J. P., Prosser, I. P., Croke, B. F. W., and Jakeman, A. J., 2003, Sensitivity analysis for assessing the behaviour of a landscape-based sediment source and transport model: Environ. Modelling Softw., v. 18, nos. 8/9, p. 741–751.

Pastres, R., Chan, K., Solidoro, C., and Dejak, C., 1999, Global sensitivity analysis of a shallow-water 3D eutrophication: Comput. Phys. Commun., v. 117, nos. 1/2, p. 62–74.

Ricotti, M. E., and Zio, E., 1999, Neural network approach to sensitivity and uncertainty analysis: Reliab. Eng. Syst. Saf., v. 64, no. 1, p. 59–71.

Rumelhart, D. E., Hinton, G. E., and Wiliams, R. H., 1986, Learning representations by back-propagating errors: Nature, v. 323, no. 9, p. 533–536.

Sung, A. H., 1998, Ranking importance of input parameters of neural networks: Expert Syst. Appl., v. 15, nos. 3/4, p. 405–411.

Wei, B., Sugiura, N., and Maekawa, T., 2001, Use of artificial neural network in the prediction of algal blooms: Water Res., v. 35, no. 8, p. 2002–2028.